

Soft Switching Symmetric Bipolar Outputs DC-Transformer (DCX) for Eliminating Power Supply Pumping of Half-Bridge Class-D Audio Amplifier

Xiang Zhou , Member, IEEE, Jianping Xu , Member, IEEE, Shu Zhong , and Yan-Fei Liu , Fellow, IEEE

Abstract—A soft switching symmetric bipolar outputs dc-transformer (DCX) for eliminating power supply pumping of half-bridge class-D audio amplifiers is proposed in this paper. Compared with the traditional unidirectional front-end dc–dc converter in the half-bridge class-D audio amplifier, output capacitances of the proposed DCX and voltage stress of the half-bridge class-D audio amplifier are significantly reduced. Soft switching of the proposed DCX can be achieved when the load current of half-bridge class-D audio amplifier is positive or negative. Thus, the efficiency and power density of the proposed audio amplifier system can be improved. In addition, the proposed DCX has smoothing transition between the positive load current and the negative load current with a simple open-loop controller. The operating principle of the proposed DCX is analyzed and a 200-W prototype is built up. Experimental results show that power supply pumping is reduced with small DCX output capacitors, symmetric bipolar outputs are obtained and peak efficiency of 96.3% is achieved.

Index Terms—DC-transformer, half-bridge class-D audio amplifier, soft switching, symmetric bipolar outputs.

I. INTRODUCTION

ALONG with the development of portable audio electronics equipment, an audio amplifier with low output voltage distortion, high efficiency, and high power-density has attracted much attention recently. Class-D audio amplifiers are thus more and more popular and start to flourish in applications where linear amplifiers once dominated [1]. Compared with linear amplifiers, modern class-D audio amplifiers benefit from small volume and high system efficiency [2].

Class-D audio amplifier can be classified into the half-bridge and full-bridge class-D audio amplifier. Compared with the full-bridge class-D audio amplifier, the half-bridge class-D audio

Manuscript received January 23, 2018; revised May 8, 2018 and July 7, 2018; accepted September 18, 2018. Date of publication September 30, 2018; date of current version May 2, 2019. Recommended for publication by Associate Editor W.-H. Ki. (*Corresponding author: Jianping Xu*)

X. Zhou, J. Xu, and S. Zhong are with the School of Electrical Engineering, Southwest Jiaotong University, Chengdu 611756, China, and also with the Key Laboratory of Magnetic Suspension Technology and Maglev Vehicle, Ministry of Education, Chengdu 611756, China (e-mail: pecel_zhouxiang@163.com; jpxu-swjtu@163.com; zhongshusky@163.com).

Y.-F. Liu is with Queen's University, Kingston, ON K7L3N6, Canada (e-mail: yanfei.liu@queensu.ca).

Color versions of one or more of the figures in this paper are available online at <http://ieeexplore.ieee.org>.

Digital Object Identifier 10.1109/TPEL.2018.2873234

amplifier has reduced devices number and stray inductance [3]. In order to provide a stable power supply for the half-bridge class-D audio amplifier system, high-performance front-end dc–dc converter is required [4]. Boost converter is used as a front-end dc–dc converter to provide unipolar supply for half-bridge class-D audio amplifier in [5]. However, a large dc blocking capacitor is required to prevent the speaker from being damaged by a high dc voltage, which reduced the power density of the audio amplifier system [6]. In contrast, in half-bridge class-D audio amplifier with bipolar power supplies, a bulky blocking capacitor can be removed [6], [7]. Typical half-bridge class-D audio amplifier system consists of front-end single input bipolar outputs dc–dc converter and half-bridge class-D audio amplifier. Bipolar outputs flyback converter or *LLC* resonant converter is widely used as a front-end converter [8], [9]. A voltage doubler rectified boost-integrated half-bridge class-D audio amplifier is proposed in [10], which achieves ZVS of switches and has no dc magnetizing current for the transformer.

Generally, due to ac load current and traditional unidirectional front-end dc–dc converter, the voltages across power supplies of half-bridge class-D audio amplifier have large voltage ripples, especially when output voltage frequency is low, which is called power supply pumping [4]. Severe power supply pumping significantly increases the voltage stress of the devices of class-D audio amplifier and deteriorates total harmonic distortion and noise (THD+N) of the audio amplifier system [11], [12]. In order to improve THD+N and suppress power supply pumping, some control strategies are studied to obtain high power supply rejection ratio (PSRR) [13]–[15]. In general, the large bulky electrolytic capacitor is used as the filter of the front-end dc–dc converter to reduce supply voltage ripple of the half-bridge class-D audio amplifier system, which reduces the power density of the audio amplifier system.

Compared with the large bulky electrolytic capacitor in a unidirectional front-end dc–dc converter, bidirectional front-end dc–dc converter can transfer feedback energy to input power supply of the audio amplifier system, which reduces the output capacitor of the dc–dc converter and increases the power density [16]. In a bidirectional dc–dc converter, soft switching and bidirectional power conversion can be achieved with some control strategies [17]–[21]. However, these converters are controlled

to operate in a forward operation mode or backward operation mode, respectively. As load current of class-D audio amplifier varies rapidly and randomly, which makes it difficult to realize soft switching by detecting the direction of the load current. Thus, these bidirectional soft switching dc–dc converters are not suitable for the class-D audio amplifier system.

As a good candidate for the front-end dc–dc converter, *LLC* resonant converter attracts much attention in decades. There are many research works on the control, common noise, and magnetics design of *LLC* converter [22]–[26]. However, due to the complex control algorithm, these converters require a microcontroller to achieve start-up and other control functions. In a bidirectional soft switching *LLC* dc–dc converter, some control strategies and circuit topologies are designed for soft switching of all the switches in forward or backward mode as well as smooth change of the output power flow direction [27]–[29]. Because maximum output frequency of audio amplifier is 20 kHz, it is difficult to design the controller of bidirectional *LLC* converter for the audio amplifier system.

In a class-D audio amplifier system, because the downstream class-D audio amplifier is close-loop and always has high PSRR, the front-end dc–dc converter can be designed as an open-loop dc-transformer (DCX) to improve the efficiency and reduce the complexity of the controller. Light load efficiency and an optimized magnetic component of the *LLC* DCX are the focus in [30]–[35]. A family of resonant DCX is proposed in [36], which achieve soft switching of switches and high system efficiency over wide load range. However, it is difficult to realize soft switching of all the switches in both forward and backward mode because these DCXs are open-loop and has fixed switching frequency as well as fixed duty cycle.

In this paper, a soft switching symmetric bipolar outputs DCX for eliminating power supply pumping of the half-bridge class-D audio amplifier is proposed. Power supply pumping of the half-bridge class-D audio amplifier is eliminated by the proposed DCX with small output capacitances, thus power supply noise and voltage stress of the devices in the half-bridge class-D audio amplifier are reduced. The proposed DCX has stable symmetric bipolar outputs with the simple open-loop controller, which significantly reduces the complexity of controller in the half-bridge class-D audio amplifier system. Soft switching of the switches in the proposed DCX can be realized when the load current of the half-bridge class-D audio amplifier is positive or negative, which improves the system efficiency.

This paper is organized as follows. Section II discusses power supply pumping and the circuit configuration of the proposed DCX. Section III contains the analysis of operation modes and performance of the proposed DCX. Sections V and VI contain experimental results and conclusion.

II. POWER SUPPLY PUMPING AND TOPOLOGY DERIVATION OF THE PROPOSED DCX

The proposed audio amplifier system, as shown in Fig. 1, consists of front-end DCX and downstream class-D audio amplifier. The proposed DCX has bidirectional power flowing path. Thus, the power supply pumping of the half-bridge class-D amplifier

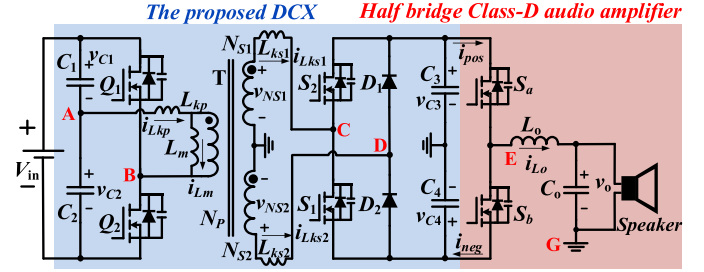


Fig. 1. Circuit diagram of the proposed audio amplifier system.

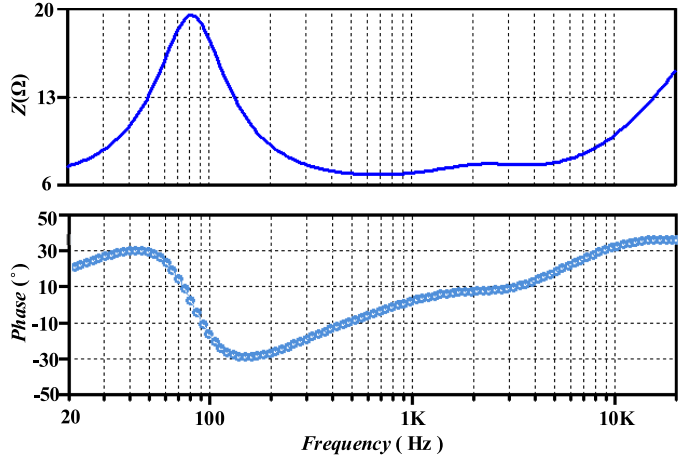


Fig. 2. Typical impedance of speaker versus different output voltage frequency of the audio amplifier.

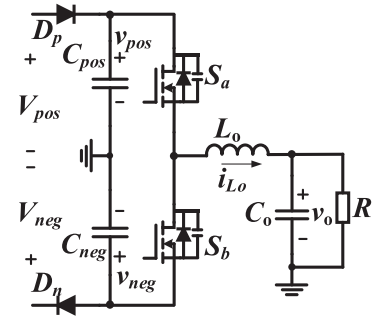


Fig. 3. Half-bridge class-D audio amplifier with a unidirectional front-end dc–dc converter.

can be reduced since a current path is provided for the reverse load current.

A. Power Supply Pumping of Half-Bridge Class-D Amplifier

Fig. 2 shows the impedance of the speaker versus the output voltage frequency of an audio amplifier. It can be observed that speaker load can be resistive, capacitive, or inductive under different output voltage frequency.

Fig. 3 shows the half-bridge class-D audio amplifier with a unidirectional front-end dc–dc converter, and the load is assumed as a resistor. Due to unidirectional power flowing paths, the reverse load current would cause output voltage pumping of the front-end dc–dc converter. Such voltages pumping

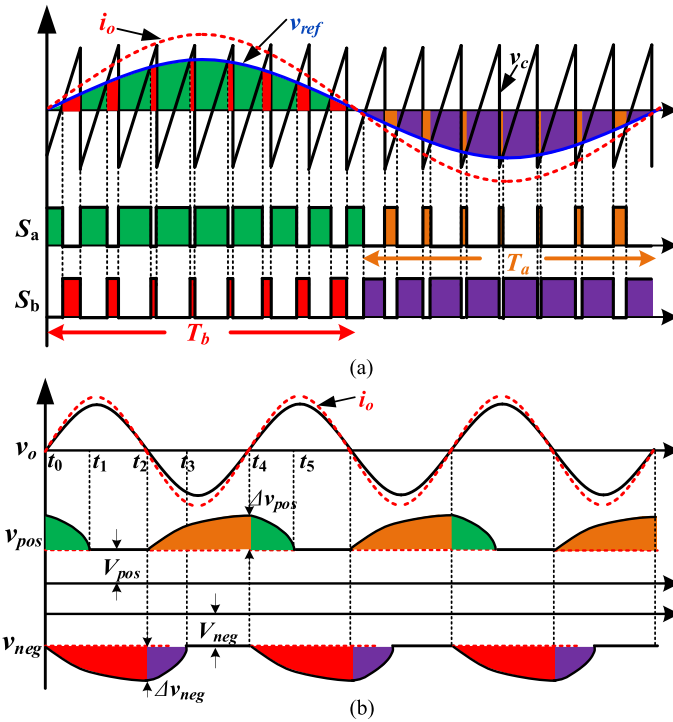


Fig. 4. Power supply pumping of half-bridge class-D audio amplifier with a unidirectional front-end dc-dc converter under resistor load. (a) Key waveforms of the half-bridge class-D audio amplifier. (b) Power supply pumping of the half-bridge class-D audio amplifier system.

increases voltage stress of switches S_a , S_b as well as capacitors C_{pos} , C_{neg} , and deteriorates the power supply noise of the half-bridge class-D audio amplifier.

Fig. 4 illustrates the power supply pumping of the half-bridge class-D audio amplifier system as shown in Fig. 3 with resistor load. In Fig. 4(a), i_o is load current of the half-bridge class-D audio amplifier, v_{ref} is audio reference voltage, and v_c is carrier. The driving signals of switches S_a and S_b are complementary, T_a is the time when load current is negative and T_b is the time when load current is positive.

For negative load current i_o , when switch S_a is turned ON and switch S_b is turned OFF, load current i_o flows from filter inductor L_o into capacitor C_{pos} through switch S_a . Thus, the charge is stored in capacitor C_{pos} , which causes bus pumping on positive power supply of the class-D audio amplifier. Because voltage v_{pos} is higher than positive power supply voltage V_{pos} , diode D_p is turned OFF. When switch S_b is turned ON and switch S_a is turned OFF, load current i_o flows from filter inductor L_o into diode D_n through switch S_b . Thus, the negative power supply of the class-D audio amplifier provides power for the load.

For positive load current i_o , when switch S_b is turned ON and switch S_a is turned OFF, load current i_o flows from switch S_b into filter inductor L_o . Thus, the charge is stored in capacitor C_{neg} , which causes bus pumping on negative power supply of the class-D audio amplifier. Because voltage v_{neg} is lower than negative power supply voltage V_{neg} , diode D_n is turned OFF. When switch S_a is turned ON and switch S_b is turned OFF, load current i_o flows from diode D_p into filter inductor L_o through

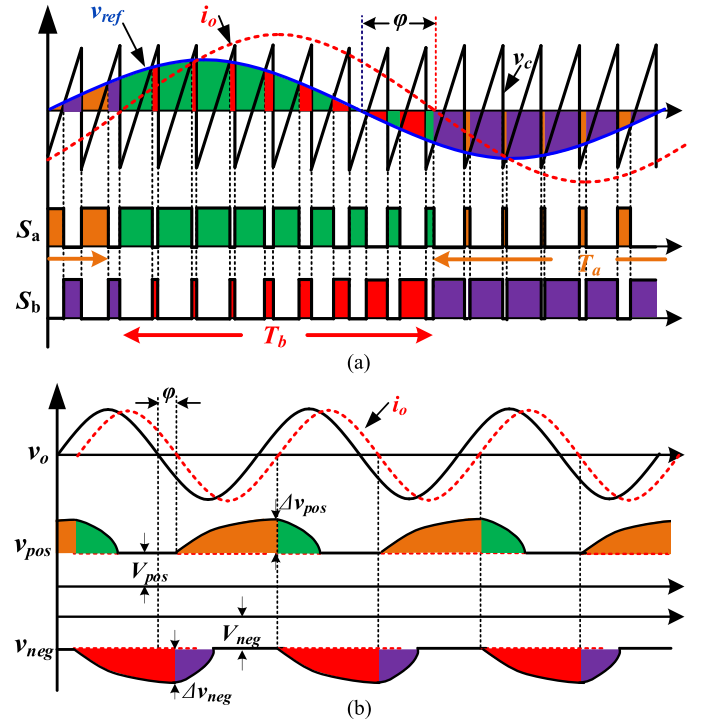


Fig. 5. Power supply pumping of the half-bridge class-D audio amplifier with a unidirectional front-end dc-dc converter under inductive load. (a) Key waveforms of the half-bridge class-D audio amplifier. (b) Power supply pumping of the half-bridge class-D audio amplifier system.

switch S_a . Thus, the positive power supply of the class-D audio amplifier provides power for the load.

As shown in Fig. 4(a), yellow area represents the time when load current i_o is negative and flows into capacitor C_{pos} through switch S_a . Red area represents the time when load current i_o is positive and flows into C_{neg} through switch S_b . Green and purple areas represent the time when positive and negative power supply provide output power for the load through switches S_a and S_b , respectively. It can be observed that the time of green area is longer than the time of yellow area and the time of purple area is longer than the time of red area.

In Fig. 4(b), V_{pos} and V_{neg} are positive and negative bus voltage for class-D audio amplifier, and Δv_{pos} and Δv_{neg} are positive and negative bus pumping voltage. As shown in Fig. 4(b), when load current i_o is positive and switch S_a is turned ON, the charge stored in capacitor C_{pos} is discharged to provide output power for the load. Thus, during the time interval t_4-t_5 , voltage v_{pos} decreases from the maximum to positive bus voltage V_{pos} . When load current i_o is negative and switch S_b is turned ON, the charge stored in capacitor C_{neg} is discharged to provide output power for the load. Thus, during the time interval t_2-t_3 , voltage v_{neg} increases from the minimum to negative bus voltage V_{neg} .

When the speaker load of the audio amplifier is inductive or capacitive, load current i_o in Fig. 4(a) will shift to the right or left. Fig. 5 illustrates the power supply pumping of the half-bridge class-D audio amplifier system as shown in Fig. 3 with an inductive load. With inductive or capacitive load, when load current i_o is negative and switch S_a is turned ON, the time of yellow area is longer than that with resistive load, which

causes more severe bus pumping on capacitor C_{pos} . Similarly, when load current i_o is positive and switch S_b is turned ON, the time of red area is longer than that with resistive load, which causes more severe bus pumping on capacitor C_{neg} . The analysis of power supply pumping of the half-bridge class-D audio amplifier system with inductive load is similar to that with resistive load.

In order to calculate the power supply pumping of the half-bridge class-D audio amplifier, setting

$$\begin{cases} v_o = mV_{\text{bus}} \sin(\omega t) \\ i_o = \frac{mV_{\text{bus}} \sin(\omega t + \varphi)}{|Z_{\text{speaker}}|} \end{cases} \quad (1)$$

where m is modulation index of class-D audio amplifier, V_{bus} is power supply voltage of the class-D audio amplifier, which equals to the magnitude of V_{pos} and V_{neg} , ω is angular frequency of output voltage of audio amplifier, φ is phase difference which the output current lags output voltage of audio amplifier, and Z_{speaker} is impedance of the speaker.

In the half-bridge class-D audio amplifier, the duty cycle of switch S_a is as follows:

$$d_{Sa} = \frac{1}{2} + \frac{1}{2}m \sin(\omega t). \quad (2)$$

As shown in Fig. 5, during T_a , load current i_o flows into capacitor C_{pos} through switch S_a , which increases the voltage across capacitor C_{pos} . If switching frequency and output voltage frequency of the class-D audio amplifier satisfy $f_s : f_o = N$, the voltage ripple across positive power supply Δv_{pos} satisfy

$$\begin{aligned} C_{\text{pos}} \cdot \Delta v_{\text{pos}} &= \int_{\frac{\pi-\varphi}{\omega}}^{\frac{2\pi-\varphi}{\omega}} -i_{Sa}(t) dt \\ &= \sum_{i=N/2}^N \left\{ -\frac{mV_{\text{pos}}}{|Z_{\text{speaker}}|} \sin\left(\frac{\omega i}{N} + \varphi\right) \right. \\ &\quad \left. \cdot \left[\frac{1}{2} + \frac{1}{2}m \sin\left(\frac{\omega i}{N}\right) \right] \right\}. \end{aligned} \quad (3)$$

When $N \rightarrow +\infty$, (3) can be rewritten as follows:

$$\begin{aligned} C_{\text{pos}} \cdot \Delta v_{\text{pos}} &= \int_{\pi}^{2\pi} -\frac{mV_{\text{pos}}}{\omega |Z_{\text{speaker}}|} \sin(x) \\ &\quad \times \left[\frac{1}{2} + \frac{1}{2}m \sin(x - \varphi) \right] dx \\ &= \frac{mV_{\text{pos}}(4 - m\pi \cos \varphi)}{4\omega |Z_{\text{speaker}}|}. \end{aligned} \quad (4)$$

Therefore, the ripple voltage across positive power supply is as follows:

$$\Delta v_{\text{pos}} = \frac{mV_{\text{pos}}(4 - m\pi \cos \varphi)}{8\pi f_o |Z_{\text{speaker}}| C_{\text{pos}}}. \quad (5)$$

Similarly, the ripple voltage across negative power supply is as follows:

$$\Delta v_{\text{neg}} = \frac{mV_{\text{pos}}(4 - m\pi \cos \varphi)}{8\pi f_o |Z_{\text{speaker}}| C_{\text{neg}}}. \quad (6)$$

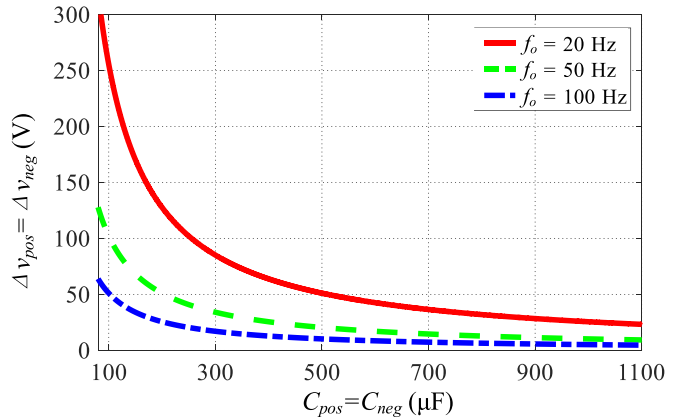


Fig. 6. Voltage ripple $\Delta v_{\text{pos}} = \Delta v_{\text{neg}}$ versus capacitances $C_{\text{pos}} = C_{\text{neg}}$.

It can be observed from (5) and (6) that when output voltage frequency of audio amplifier is low, power supply pumping is severe. Assume that $m = 0.7$, $V_{\text{pos}} = 35$ V, $Z_{\text{load}} = 4$ Ω and $\varphi = \pi/6$, according to (5) and (6), Fig. 6 shows the relationship between $\Delta v_{\text{pos}} = \Delta v_{\text{neg}}$ and capacitances $C_{\text{pos}} = C_{\text{neg}}$. As shown in Fig. 6, if $f_o = 20$ Hz, $\Delta v_{\text{pos}} = \Delta v_{\text{neg}} = 35$ V, large capacitors $C_{\text{pos}} = C_{\text{neg}} = 731.1$ μF with 70 V voltage stress are needed. If smaller voltage ripple $\Delta v_{\text{pos}} = \Delta v_{\text{neg}}$ is required, it has to increase capacitances $C_{\text{pos}} = C_{\text{neg}}$, which reduces power density of the audio amplifier system.

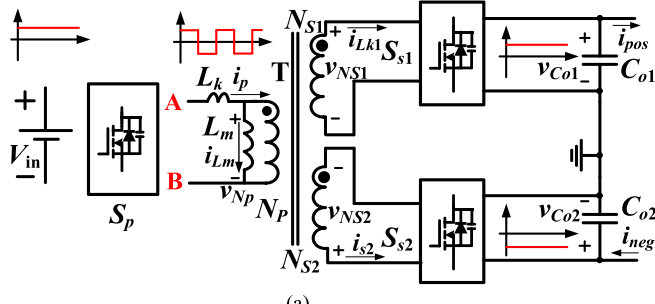
If the diodes D_p and D_n in Fig. 3 are replaced by switches and bidirectional current flowing path is provided for the half-bridge class-D audio amplifier, the charge can be transferred instead of stored in the capacitors C_{pos} and C_{neg} , thus power supply pumping can be eliminated.

B. Topology Derivation of the Proposed DCX

Half-bridge circuit, full-bridge circuit, push-pull circuit, two-switch forward circuit, etc., can be used in transformer primary to generate square wave voltage with 0.5 duty cycle. Fig. 7 shows the circuit configuration of the proposed DCX. When square wave with a constant duty cycle is generated in the transformer primary, the proposed DCX can generate constant positive and negative output voltages when a full-wave or full-bridge rectifier is adopted in transformer secondary. Thus, if the leakage inductance of the transformer is neglected, the bipolar output voltages of the proposed DCX are always clamped by the input voltage of the DCX. Therefore, the voltage ripples across outputs of the proposed DCX are theoretically zero, even if output capacitors of the DCX are zero. Thus, the output filter of the DCX is reduced, and the power density of the proposed audio amplifier system can be improved.

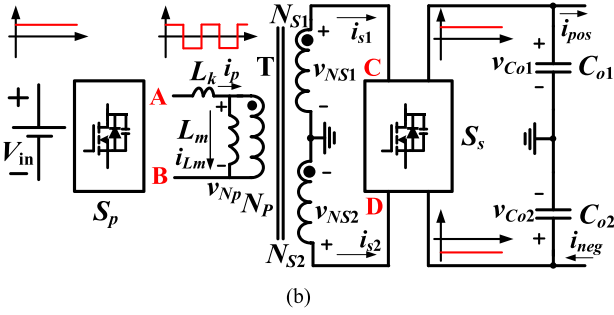
In Fig. 7, in order to generate symmetric bipolar outputs, two full-bridge rectifiers are necessary to ensure constant output voltages in type I DCX, as shown in Fig. 7(a). Compared with type II DCX as shown in Fig. 7(b), type I DCX needs more rectifier diodes or switches. Thus, type II DCX with half-bridge circuit in the transformer primary is adopted.

Fig. 8 shows four kinds of the rectifier. Front-end bidirectional dc-dc converter is required to reduce power supply pumping in



(a)

(b)



(b)

Fig. 7. Circuit configuration of the proposed DCX. (a) Type I. (b) Type II.

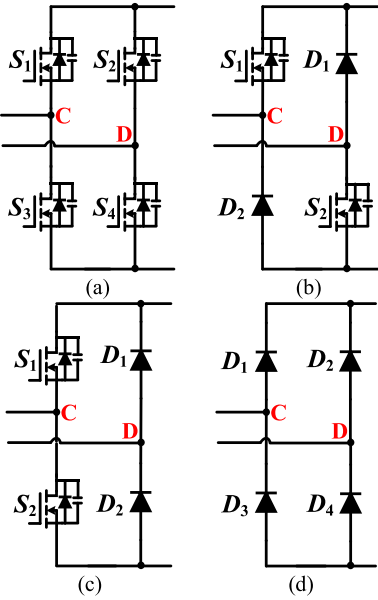
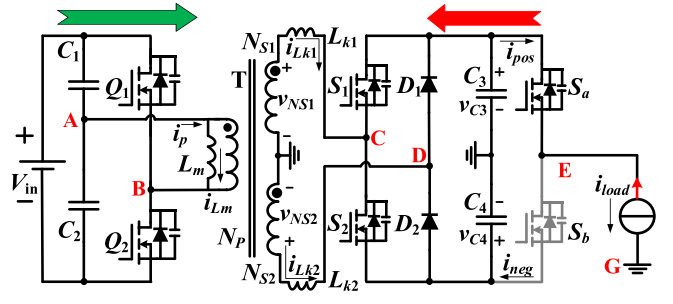


Fig. 8. Circuit diagram of rectifier.

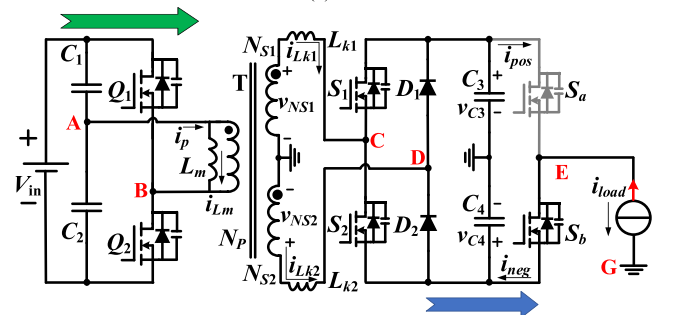
the half-bridge class-D audio amplifier and provide a path for the reserve load current. The rectifier as shown in Fig. 8(c) is adopted in the proposed DCX due to bidirectional power conversion with less active devices.

III. ANALYSIS OF OPERATION MODES AND CHARACTERISTIC OF THE PROPOSED DCX

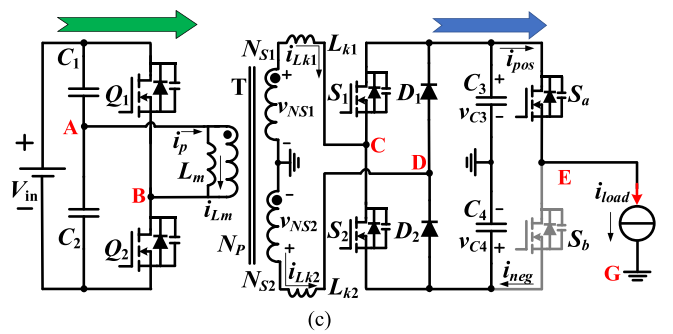
In this paper, the proposed DCX is connected to the half-bridge class-D audio amplifier. For an audio amplifier, the load current is ac and the frequency range of load current is 20 Hz–20 kHz, which is much lower than the switching frequency of



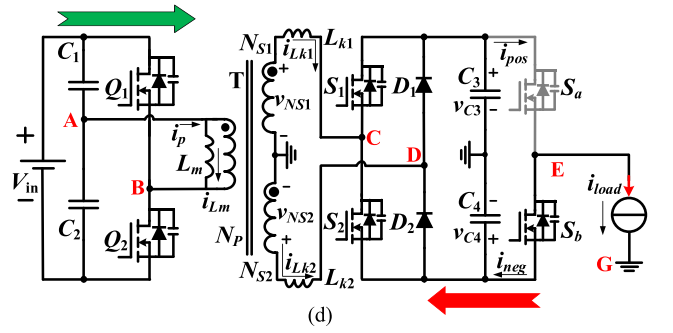
(a)



(b)



(c)



(d)

Fig. 9. Circuit diagram of power flow in the proposed DCX. (a) Negative load current of the class-D audio amplifier when switch S_a is turned ON. (b) Negative load current of the class-D audio amplifier when switch S_b is turned ON. (c) Positive load current of class-D audio amplifier when switch S_a is turned ON. (d) Positive load current of class-D audio amplifier when switch S_b is turned ON.

the proposed DCX. Therefore, in one switching period of the proposed DCX, the load current of the half-bridge class-D audio amplifier can be regarded as constant since filter inductor is large and ripple current of filter inductor is small.

Fig. 9 shows the circuit diagram of power flow in the proposed DCX. As shown in Fig. 9(a), for negative load current, when switch S_a is turned ON, current i_{load} flows from switch S_a to

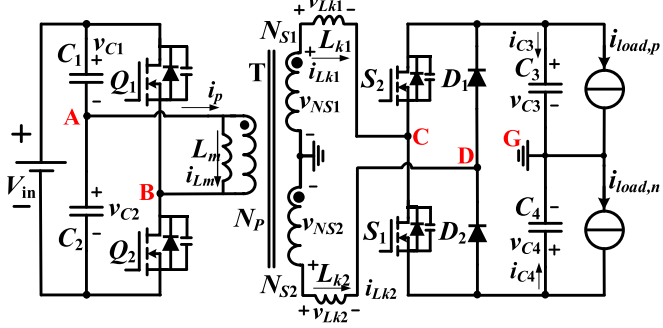
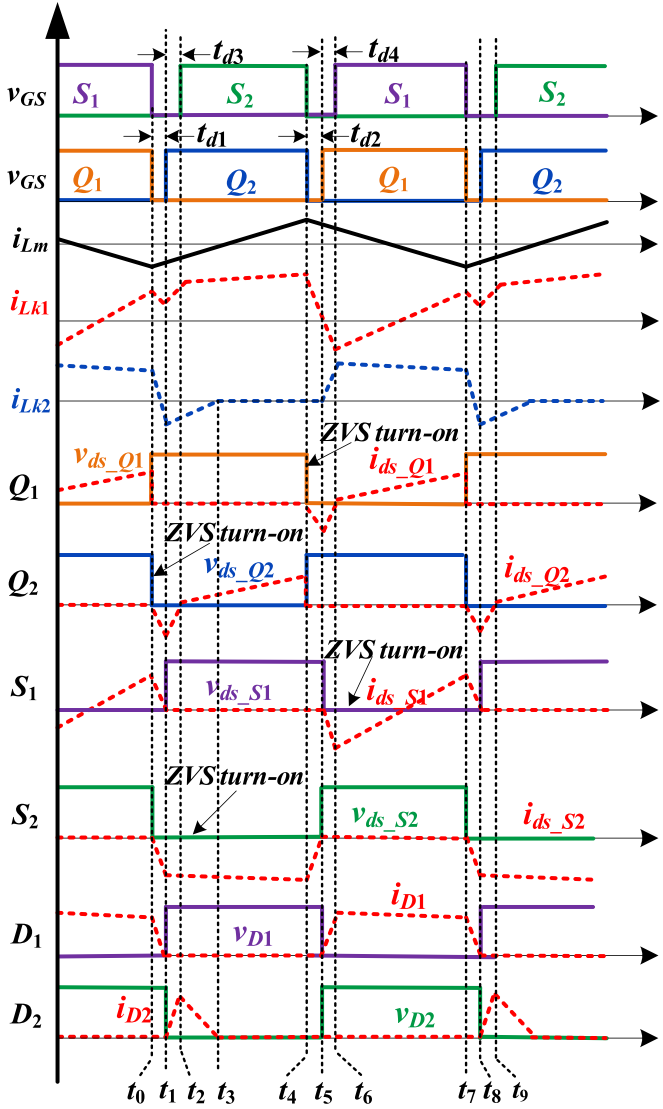


Fig. 10. Equivalent circuit of the proposed DCX.

Fig. 11. Key waveforms of the proposed DCX when currents $i_{load,p} > 0$ and $i_{load,n} < 0$.

capacitor C_3 and positive bus is charged. Therefore, the power is returned to positive bus. As shown in Fig. 9(b), for negative load current, when switch S_b is turned ON, current i_{load} flows from switch S_b to capacitor C_4 . Therefore, the power is consumed by the load. As shown in Fig. 9(c), for positive load current, when switch S_a is turned ON, current i_{load} flows from capacitor C_3 to

switch S_a . Therefore, the power is consumed by the load. As shown in Fig. 9(d), for positive load current, when switch S_b is turned ON, current i_{load} flows from capacitor C_4 to switch S_b and negative bus is discharged. Therefore, the power is returned to negative bus.

As shown in Fig. 5(a), if $-90^\circ < \varphi < 90^\circ$, the time of green area is longer than the time of yellow area, and the time of purple area is longer than the time of red area, which means that the conduction time of switch S_b is longer than that of switch S_a when current i_{load} is negative, and the conduction time of switch S_a is longer than that of switch S_b when current i_{load} is positive. Thus, the average power of the proposed DCX is positive when the load current is positive or negative. In the proposed DCX, positive and negative outputs have bidirectional power, input port has unidirectional power. For positive output, the feedback energy can be consumed by the negative output, and for negative output, the feedback energy can be consumed by the positive output.

In order to ensure low-distortion of the output voltage at 20 kHz or even higher audio signal frequency, the switching frequency of class-D audio amplifier is generally very high. As the switching frequency of class-D audio amplifier is higher than the switching frequency of the proposed DCX, when the operation mode of the proposed DCX is analyzed, the load current can be regarded as two average equivalent current sources for the positive and negative bus. The average equivalent current sources $i_{load,p}$ and $i_{load,n}$ satisfy

$$\begin{cases} i_{load,p}(t) = d_{Sa} i_{load} = d_{Sa} i_o \\ i_{load,n}(t) = d_{Sb} i_{load} = d_{Sb} i_o. \end{cases} \quad (7)$$

From (1), (2), and (7), average equivalent current sources $i_{load,p}$ and $i_{load,n}$ are as follows:

$$\begin{cases} i_{load,p}(t) = [\frac{1}{2} + \frac{1}{2}m \sin(\omega t)] \frac{m V_{bus} \sin(\omega t + \varphi)}{|Z_{speaker}|} \\ i_{load,n}(t) = -[\frac{1}{2} - \frac{1}{2}m \sin(\omega t)] \frac{m V_{bus} \sin(\omega t + \varphi)}{|Z_{speaker}|}. \end{cases} \quad (8)$$

In order to simplify the analysis of the proposed DCX as shown in Fig. 2, assume that all power switches are ideal except their body diode and output capacitances C_{oss} , the output capacitances of all switches are the same, and the diodes are ideal. Fig. 10 shows the equivalent circuit of the proposed DCX connected half-bridge class-D audio amplifier.

A. Operation Modes of the Proposed DCX When Load Current of Class-D Audio Amplifier is Positive

When load current of the half-bridge class-D audio amplifier is positive, currents $i_{load,p}$ and $i_{load,n}$ satisfy $i_{load,p} > 0$ and $i_{load,n} < 0$ in the equivalent circuit of the proposed DCX. Fig. 11 shows the key waveforms of the proposed DCX. As shown in Fig. 11, t_{d1} and t_{d2} are the dead time of primary side half-bridge circuit. If t_{d1} and t_{d2} are neglected, the driving signals of switches $Q1$ and $Q2$ are complementary with constant duty cycle 0.5. In order to ensure soft switching of switches $S1-S2$, the turn-ON of switches $S1$ and $S2$ should lag behind the turn-ON of switch $Q1$ and $Q2$ with a delay time t_{d3} and t_{d4} . If dead time and delay time are neglected, the driving signals of switches

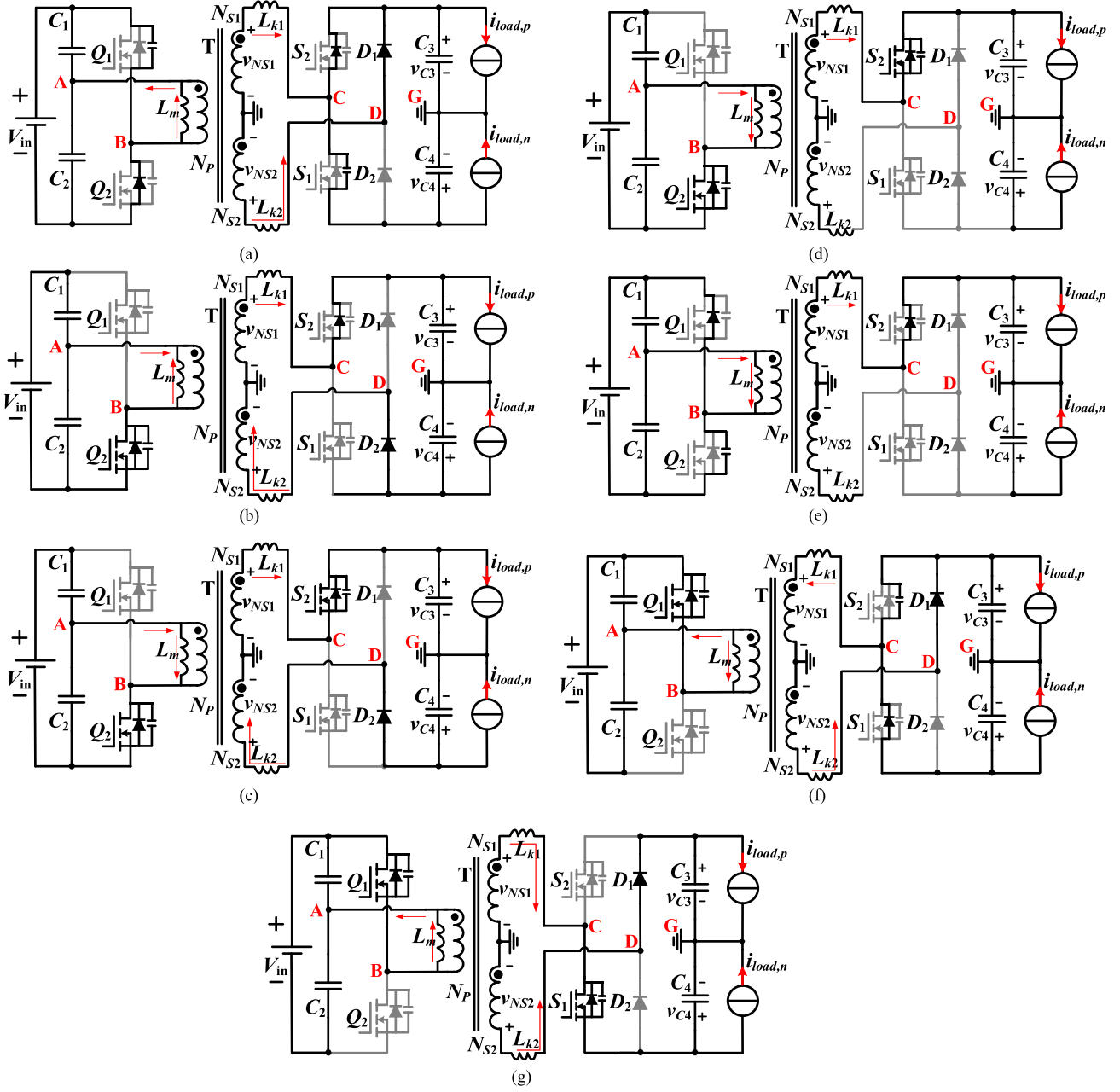


Fig. 12. Operation mode of the proposed DCX when currents $i_{load,p} > 0$ and $i_{load,n} < 0$. (a) Mode 1 (t_0-t_1). (b) Mode 2 (t_1-t_2). (c) Mode 3 (t_2-t_3). (d) Mode 4 (t_3-t_4). (e) Mode 5 (t_4-t_5). (f) Mode 6 (t_5-t_6). (g) Mode 7 (t_6-t_7).

$S1$ and $S2$ are complementary with constant duty cycle 0.5. In steady state, the proposed DCX has seven operation modes as shown in Fig. 12.

Mode 1 [t_0-t_1]: At t_0 , switches Q_1 and S_1 are turned OFF, the proposed DCX operates in dead time mode. After switches Q_1 and S_1 are turned OFF, the output capacitor of switch Q_1 is charged and the output capacitor of switch Q_2 is discharged. Voltage across node A and node B v_{AB} changes from negative to positive, thus current i_{LK2} decreases. The body diode of switch S_2 is conducted to provide current flowing paths for the free-wheeling of secondary leakage inductance current i_{LK1} . When the output capacitor of switch Q_2 is completely discharged,

the body diode of switch Q_2 is conducted and ZVS turn-ON of switch Q_2 can be achieved. This mode is short and ends when switch Q_2 is turned ON at t_1 .

To ensure ZVS turn-ON of switch Q_2 , it should have

$$\frac{1}{2} \frac{L_{k1} + L_{k2}}{4n^2} [-ni_{LK1}(t_0) + ni_{LK2}(t_0) - i_{Lm}(t_0)]^2 + \frac{1}{2} L_m i_{Lm}(t_0)^2 > \frac{1}{2} (C_{oss,Q1} + C_{oss,Q2}) V_{in}^2. \quad (9)$$

It can be observed from (9), L_m is much larger than L_{k1} and L_{k2} , and ZVS turn-ON of switch Q_2 can be achieved easily. If ZVS turn-ON of switch Q_2 can be achieved in dead time

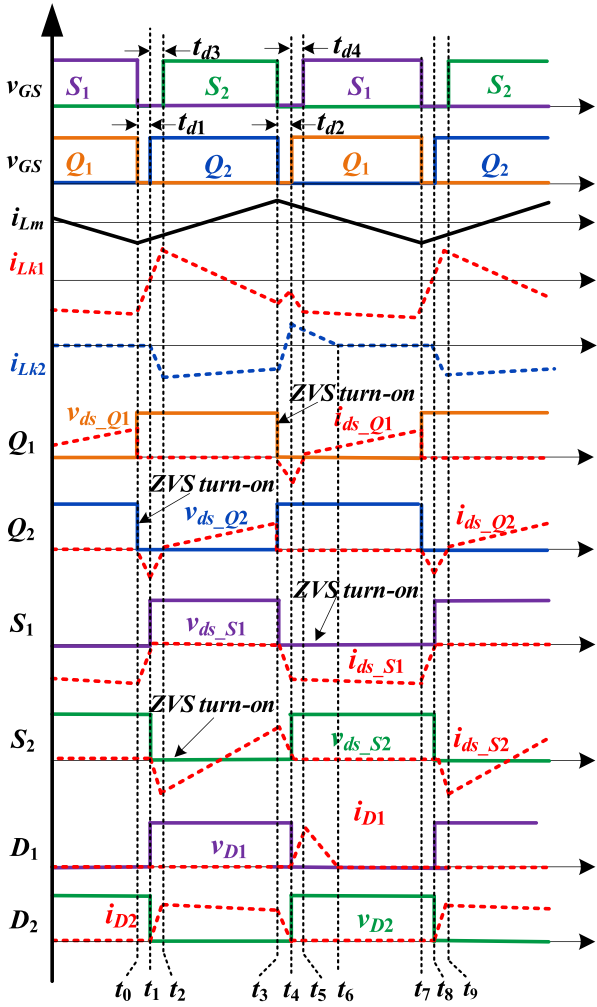


Fig. 13 Key waveforms of the proposed DCX when currents $i_{\text{load},p} < 0$ and $i_{\text{load},n} > 0$.

$t_{d1}, t_{d1} = t_1 - t_0$ should satisfy

$$\int_{t_0}^{t_1} [-ni_{Lk1} + ni_{Lk2} - i_{Lm}] dt > (C_{\text{oss},Q1} + C_{\text{oss},Q2})V_{\text{in}}. \quad (10)$$

Because current i_{Lm} can be regarded as constant during t_{d1} , (10) can be approximated and rewritten as follows:

$$-i_{Lm}(t_0)t_{d1} = \frac{V_{\text{in}}T}{4L_m}t_{d1} > (C_{\text{oss},Q1} + C_{\text{oss},Q2})V_{\text{in}}. \quad (11)$$

Mode 2 [t_1-t_2]: At t_1 , switch Q_2 is turned ON, and the proposed DCX operates in delay time mode. In this mode, because voltage v_{AB} is positive, current i_{LK1} is positive and current i_{LK2} is negative, the body diode of S_2 and diode D_2 are conducted to provide current flowing paths for currents i_{LK1} and i_{LK2} . This mode is short and ends when switch S_2 is turned ON at t_2 .

Mode 3 [t_2-t_3]: At t_2 , switch S_2 achieves ZVS turn-ON. In this mode, because the load current $i_{\text{load},p}$ is positive and the load current $i_{\text{load},n}$ is negative, the input power supply provides power for positive output through leakage inductance L_{k1} and switch S_2 .

In this mode, because the load current $i_{\text{load},n}$ is negative, voltage v_{C4} decreases and is lower than v_{NS2} . Current i_{LK2}

increases from negative to zero, and diode D_2 achieves ZCS turn-OFF. This mode ends when diode D_2 is turned OFF at t_3 .

Mode 4 [t_3-t_4]: At t_3 , diode D_2 is turned OFF. In this mode, switches Q_2 and S_2 are conducted. Current i_{LK1} still flows from switch S_2 to capacitor C_3 . This mode ends when switches Q_2 and S_2 are turned OFF at t_4 .

Mode 5 [t_4-t_5]: At t_4 , switches Q_2 and S_2 are turned OFF. The proposed DCX operates in dead time mode. After switches Q_2 and S_2 are turned OFF, the output capacitor of switch Q_2 is charged and the output capacitor of switch Q_1 is discharged. Voltage across node A and node B v_{AB} changes from positive to negative, thus current i_{LK1} decreases sharply. The body diode of switch S_2 is still conducted when current i_{LK1} is positive. When the output capacitor of switch Q_1 is completely discharged, the body diode of switch Q_1 is conducted and ZVS turn-ON of switch Q_1 can be achieved. This mode is short and ends when switch Q_1 is turned ON at t_5 .

To ensure ZVS turn-ON of switch Q_1 , it should have

$$\begin{aligned} \frac{1}{2} \frac{L_{k1} + L_{k2}}{4n^2} [ni_{Lk1}(t_4) + i_{Lm}(t_4)]^2 + \frac{1}{2} L_m i_{Lm}(t_4)^2 \\ > \frac{1}{2} (C_{\text{oss},Q1} + C_{\text{oss},Q2}) V_{\text{in}}^2. \end{aligned} \quad (12)$$

It can be observed from (12), L_m is much larger than L_{k1} and L_{k2} , and ZVS turn-ON of switch Q_1 can be achieved easily. If ZVS turn-ON of switch Q_1 can be achieved in dead time $t_{d2}, t_{d2} = t_5 - t_4$ should satisfy

$$\int_{t_4}^{t_5} [ni_{Lk1} + i_{Lm}] dt > (C_{\text{oss},Q1} + C_{\text{oss},Q2}) V_{\text{in}}. \quad (13)$$

Because current i_{Lm} can be regard as constant during t_{d2} , (13) can be approximated and rewritten as follows:

$$i_{Lm}(t_4)t_{d2} = \frac{V_{\text{in}}T}{4L_m}t_{d2} > (C_{\text{oss},Q1} + C_{\text{oss},Q2}) V_{\text{in}}. \quad (14)$$

Mode 6 [t_5-t_6]: At t_5 , switch Q_1 is turned ON, and the proposed DCX operates in delay time mode. Current i_{LK1} decreases to negative and current i_{LK2} is positive. In this mode, the body diode of S_1 and diode D_1 are conducted to provide current flowing paths for currents i_{LK1} and i_{LK2} . This mode is short and ends when switch S_1 is turned ON at t_6 .

Mode 7 [t_6-t_7]: At t_6 , switch S_1 achieves ZVS turn-ON. Because the load current $i_{\text{load},p}$ is positive and the load current $i_{\text{load},n}$ is negative. In this mode, the input power supply provides power for positive output through leakage inductance L_{k2} and diode D_1 .

Because the load current $i_{\text{load},n}$ is negative and capacitor C_4 is discharged in mode 3 as shown in Fig. 12, current i_{LK1} increases from negative to positive and flows form switch S_1 to capacitor C_4 to balance the charge of capacitor C_4 in this mode. This mode ends when switches Q_1 and S_1 are turned OFF at t_7 .

B. Operation Modes of the Proposed DCX When Load Current of Class-D Audio Amplifier is Negative

When load current of the half-bridge class-D audio amplifier is negative, currents $i_{\text{load},p}$ and $i_{\text{load},n}$ satisfy $i_{\text{load},p} < 0$ and $i_{\text{load},n} > 0$ in the equivalent circuit of the proposed DCX. Fig. 13 shows the key waveforms of the proposed DCX. As shown in

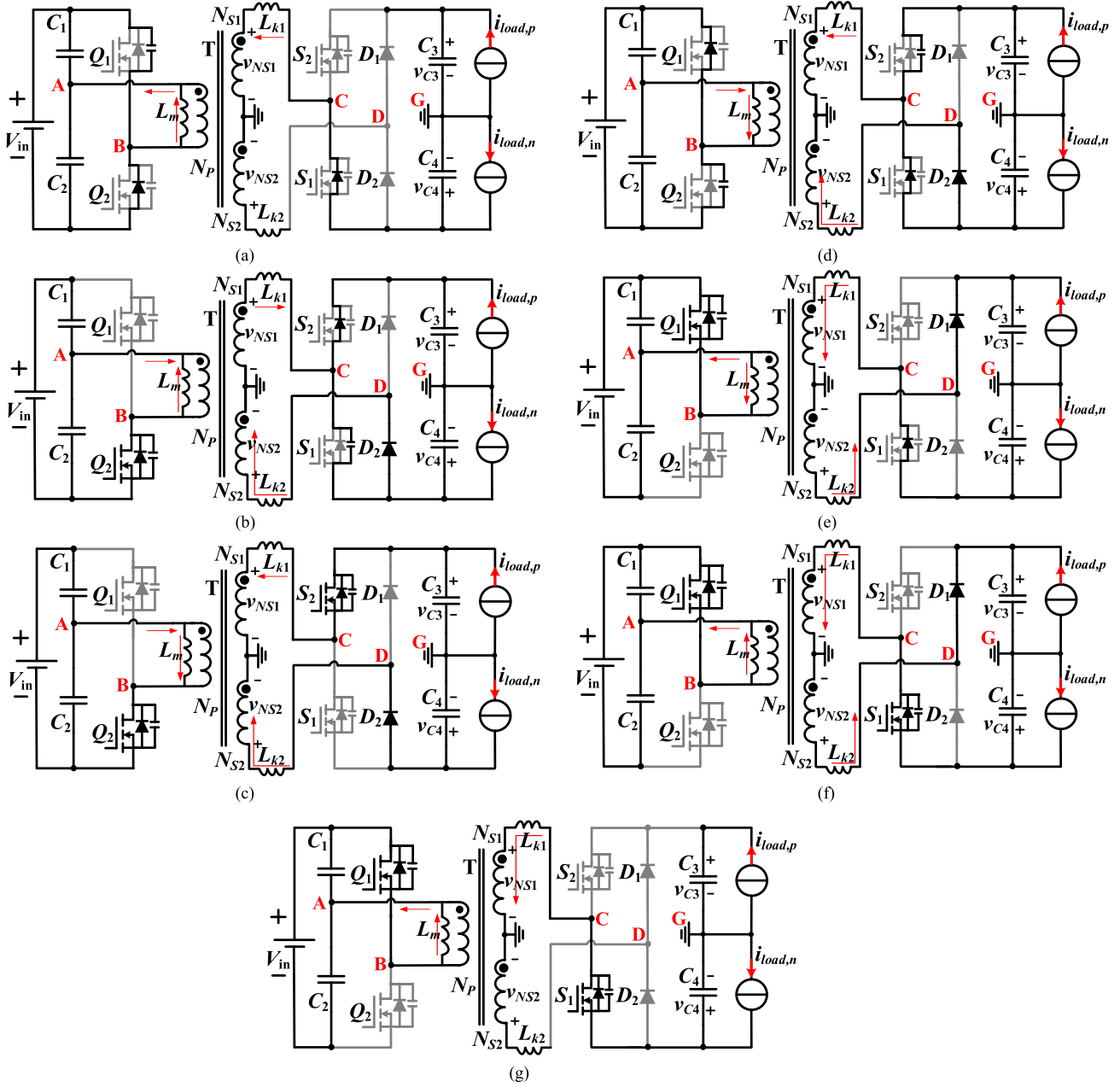


Fig. 14. Operation mode of the proposed DCX. (a) Mode 1 (t_0-t_1). (b) Mode 2 (t_1-t_2). (c) Mode 3 (t_2-t_3). (d) Mode 4 (t_3-t_4). (e) Mode 5 (t_4-t_5). (f) Mode 6 (t_5-t_6). (g) Mode 7 (t_6-t_7).

Fig. 13, t_{d1} and t_{d2} are the dead time of the primary side half-bridge circuit. If t_{d1} and t_{d2} are neglected, the driving signals of switches Q_1 and Q_2 are complementary with constant duty cycle 0.5. In order to ensure soft switching of switches S_1-S_2 , the turn-ON of switches S_1 and S_2 lags behind the turn-ON of switch Q_1 and Q_2 with a delay time t_{d3} and t_{d4} . If t_{d3} and t_{d4} are neglected, the driving signals of switches S_1 and S_2 are complementary with constant duty cycle 0.5. In steady state, the proposed DCX has seven operation modes as shown in Fig. 14.

Mode 1 [t_0-t_1]: At t_0 , switches Q_1 and S_1 are turned OFF, the proposed DCX operates in dead time mode. After switches Q_1 and S_1 are turned OFF, the output capacitor of switch Q_1 is charged and the output capacitor of switch Q_2 is discharged.

Voltage across node A and node B v_{AB} changes from negative to positive, thus current i_{LK1} increases sharply. The body diode of switch S_1 is still conducted when current i_{LK1} is negative. When the output capacitor of switch Q_2 is completely discharged, the body diode of switch Q_2 is conducted and ZVS turn-ON of switch Q_2 can be achieved. This mode is short and ends when switch Q_2 is turned ON at t_1 .

To ensure ZVS turn-ON of switch Q_2 , it should have

$$\frac{1}{2} \frac{L_{k1} + L_{k2}}{4n^2} [-ni_{LK1}(t_0) - i_{Lm}(t_0)]^2 + \frac{1}{2} L_{m} i_{Lm}(t_0)^2 > \frac{1}{2} (C_{oss,Q1} + C_{oss,Q2}) V_{in}^2. \quad (15)$$

It can be observed from (15), L_m is much larger than L_{k1} and L_{k2} , and ZVS turn-ON of switch Q_1 can be achieved easily. If ZVS turn-ON of switch Q_1 can be achieved in dead time t_{d1} , $t_{d1} = t_1 - t_0$ should satisfy

$$\int_{t_0}^{t_1} [-ni_{Lk1} - i_{Lm}] dt > (C_{oss,Q1} + C_{oss,Q2})V_{in}. \quad (16)$$

Because current i_{Lm} can be regard as constant during t_{d1} , (16) can be approximated and rewritten as follows:

$$-i_{Lm}(t_0)t_{d1} = \frac{V_{in}T}{4L_m}t_{d1} > (C_{oss,Q1} + C_{oss,Q2})V_{in}. \quad (17)$$

Mode 2 [t₁–t₂]: At t_1 , switch Q_2 is turned ON, and the proposed DCX operates in delay time mode. In this mode, because voltage v_{AB} is positive, current i_{LK1} increases to positive and current i_{LK2} is negative, the body diode of S_2 and diode D_2 are conducted to provide current flowing paths for currents i_{LK1} and i_{LK2} . This mode is short and ends when switch S_2 is turned ON at t_2 .

Mode 3 [t₂–t₃]: At t_2 , switch S_2 achieves ZVS turn-ON. In this mode, because the load current $i_{load,n}$ is positive and the load current $i_{load,p}$ is negative, the input power supply provides power for negative output through leakage inductance L_{k2} and diode D_2 .

Because the load current $i_{load,p}$ is negative and capacitor C_3 is charged in mode 6 as shown in Fig. 14, current i_{LK1} decreases from positive to negative and flows from capacitor C_3 to switch S_2 to balance the charge of capacitor C_4 in this mode. This mode ends when switches Q_2 and S_2 are turned OFF at t_3 .

Mode 4 [t₃–t₄]: At t_3 , switches Q_2 and S_2 are turned OFF. The proposed DCX operates in dead time mode. After switches Q_2 and S_2 are turned OFF, the output capacitor of switch Q_2 is charged and the output capacitor of switch Q_1 is discharged. Voltage across node A and node B v_{AB} changes from positive to negative, thus current i_{LK2} increases sharply. The body diode of S_1 is conducted to provide current flowing paths for currents i_{LK1} and the diode D_2 is still conducted when current i_{LK1} is negative. When the output capacitor of switch Q_1 is completely discharged, the body diode of switch Q_1 is conducted and ZVS turn-ON of switch Q_1 can be achieved. This mode is short and ends when switch Q_1 is turned ON at t_4 .

To ensure ZVS turn-ON of switch Q_1 , it should have

$$\begin{aligned} \frac{1}{2} \frac{L_{k1} + L_{k2}}{4n^2} [-ni_{Lk1}(t_3) + ni_{Lk2}(t_3) + i_{Lm}(t_3)]^2 \\ + \frac{1}{2} L_m i_{Lm}(t_3)^2 > \frac{1}{2} (C_{oss,Q1} + C_{oss,Q2}) V_{in}^2. \end{aligned} \quad (18)$$

It can be observed from (18), L_m is much larger than L_{k1} and L_{k2} , and ZVS turn-ON of switch Q_2 can be achieved easily. If ZVS turn-ON of switch Q_2 can be achieved in dead time t_{d2} , $t_{d2} = t_4 - t_3$ should satisfy

$$\int_{t_3}^{t_4} [-ni_{Lk1} + ni_{Lk2} + i_{Lm}] dt > (C_{oss,Q1} + C_{oss,Q2})V_{in}. \quad (19)$$

Because current i_{Lm} can be regard as constant during t_{d2} , (19) can be approximated and rewritten as follows:

$$i_{Lm}(t_4)t_{d2} = \frac{V_{in}T}{4L_m}t_{d2} > (C_{oss,Q1} + C_{oss,Q2})V_{in}. \quad (20)$$

Mode 5 [t₄–t₅]: At t_4 , switch Q_1 is turned ON, and the proposed DCX operates in delay time mode. Current i_{LK1} is negative and current i_{LK2} is positive. In this mode, the body diode of S_1 and diode D_1 are conducted to provide current flowing paths for currents i_{LK1} and i_{LK2} . This mode is short and ends when switch S_1 is turned ON at t_5 .

Mode 6 [t₅–t₆]: At t_5 , switch S_1 achieves ZVS turn-ON. Because the load current $i_{load,p}$ is negative and the load current $i_{load,n}$ is positive. In this mode, the input power supply provides power for negative output through leakage inductance L_{k1} and switch S_1 .

In this mode, because the load current $i_{load,p}$ is negative, voltage v_{C3} increases and is higher than v_{NS2} . Current i_{LK2} decreases from positive to zero, and diode D_1 achieves ZCS turn-OFF. This mode ends when diode D_1 is turned OFF at t_6 .

Mode 7 [t₆–t₇]: At t_6 , diode D_1 is turned OFF. In this mode, switches Q_1 and S_1 are conducted. Current i_{LK1} still flows from capacitor C_4 to switch S_1 . This mode ends when switches Q_1 and S_1 are turned OFF at t_7 .

C. Characteristic Analysis of the Proposed DCX

In the positive or negative half ac output current cycle of the class-D audio amplifier, dead times t_{d1} and t_{d2} , as well as delay times t_{d3} and t_{d4} are very short. If t_{d1}, t_{d2}, t_{d3} , and t_{d4} are neglected, according to volte-second balance of L_{k1} , it has

$$\int_0^{\frac{T}{2}} \left[\frac{nV_{in}}{2} - v_{C3}(t) \right] = \int_{\frac{T}{2}}^T \left[\frac{nV_{in}}{2} + v_{C4}(t) \right]. \quad (21)$$

From (21), there is

$$\int_0^{\frac{T}{2}} v_{C3}(t) = - \int_{\frac{T}{2}}^T v_{C4}(t). \quad (22)$$

According to (22), if voltage ripples across capacitors C_3 and C_4 are small, then the average voltage V_{C3} is equal to $-V_{C4}$. Thus, output voltages of the proposed DCX is symmetric no matter what load current, which is suitable for providing bipolar supplies for the half-bridge class-D audio amplifier.

As shown in Fig. 15, the current flowing through a transformer of the *LLC* dc–dc converter and the voltage across output capacitor of the dual active bridge dc–dc converter are high-frequency pulsating. Therefore, a large capacitor is required to provide a stable output voltage in the two kinds of dc–dc converters.

In the proposed DCX, as shown in Fig. 10, if the leakage inductance of transformer, dead time and delay time as well as communication of switches are neglected, positive output voltage and negative output voltage are constant even without output capacitors because the driving signals of switches Q_1 and Q_2 are complementary with constant duty cycle 0.5 and the driving signals of switches S_1 and S_2 are complementary with constant duty cycle 0.5. The ideal equivalent circuit of the proposed DCX is shown in Fig. 16. The proposed DCX has

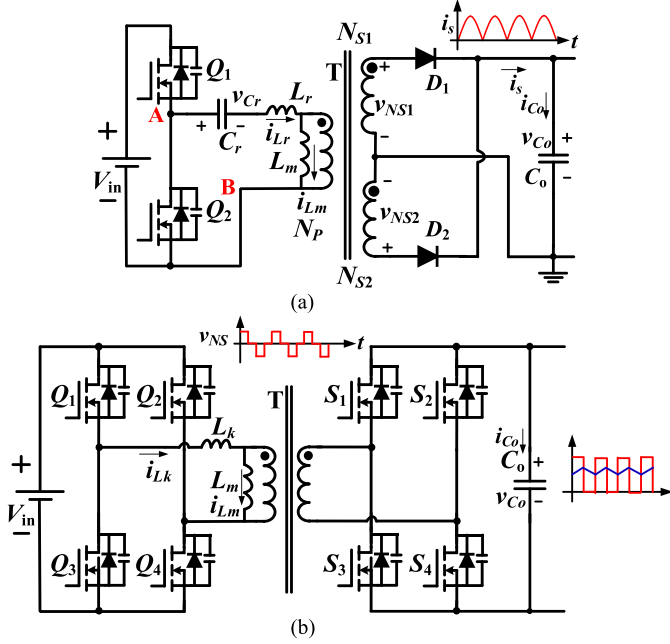


Fig. 15. Circuit diagram of the LLC dc-dc converter and the dual active bridge dc-dc converter. (a) LLC dc-dc converter in [34]. (b) Dual active bridge dc-dc converter in [21].

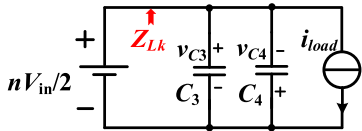


Fig. 16. Ideal equivalent circuit of the proposed DCX.

smooth transition between positive and negative current i_{load} because input supply can be regarded as voltage source. When the switches and diodes are ideal, the leakage inductances and dead time $t_{d1}-t_{d2}$ as well as delay time $t_{d3}-t_{d4}$ are neglected, voltages v_{C3} and v_{C4} have no ripples. Then bipolar outputs voltage of the proposed DCX are as follows:

$$V_{C3} = -V_{C4} = \frac{nV_{in}}{2}. \quad (23)$$

In the proposed DCX, the leakage inductance L_{k2} is connected with diodes D_1 or D_2 , and current i_{LK2} has CCM and DCM due to complex ac load current of the half-bridge class-D audio amplifier. Generally, leakage inductances are small and have limited effect on outputs voltage gains. As shown in Fig. 17, simulation positive and negative outputs voltage gains are given with different leakage inductances and load current by PSIM software. According to (8), the equivalent load current of the proposed DCX depends on modulation index m when $Z_{speaker} = 4\Omega$, $\varphi = 0$, $\sin(\omega t) = 1$, and $V_{bus} = 54$ V. It can be seen that outputs voltage gains can be regard as constant when leakage inductances are $L_{k1} = L_{k2} = L_k = 0.35$ μ H.

The comparison between the proposed DCX and some other front-end dc-dc converters for the class-D audio amplifier is summarized in Table I. It can be observed from Table I, the proposed DCX has a simple controller, small output capacitors,

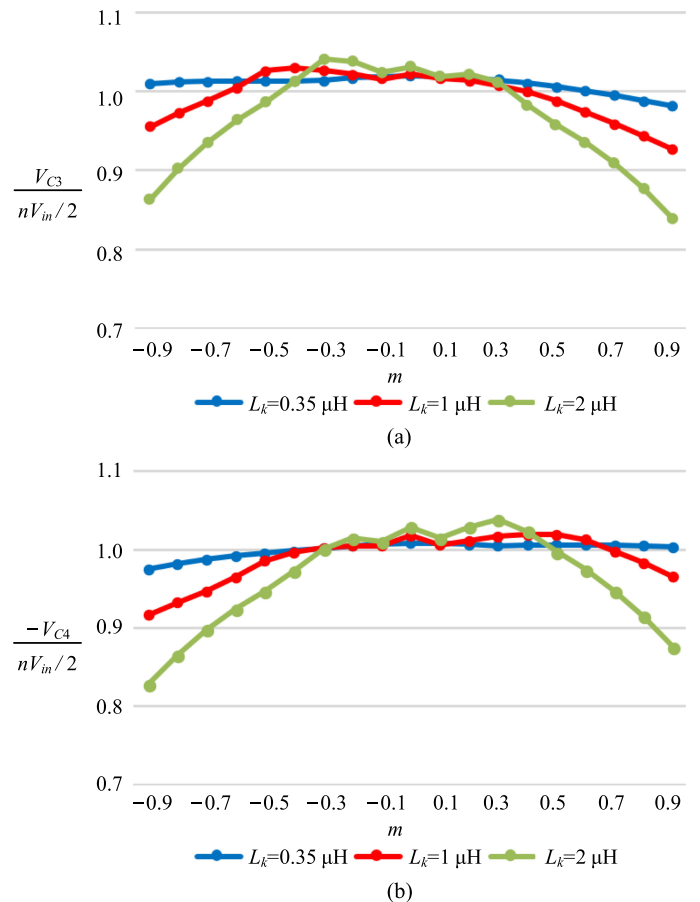


Fig. 17. Outputs voltage gains versus modulation index m under different $L_{k1} = L_{k2} = L_k$. (a) $(V_{C3})/(nV_{in}/2)$. (b) $(-V_{C4})/(nV_{in}/2)$.

and soft switching of all the switches with bidirectional load current.

IV. EXPERIMENTAL RESULTS

To verify the analysis results of the proposed DCX, a 200-W prototype is implemented. The circuit diagram is shown in Fig. 18. Because in the half-bridge class-D audio amplifier system, the class-D audio amplifier is close-loop and has high PSRR, the proposed DCX is open-loop and provide a probable bus voltage for the class-D audio amplifier. Thus, rectified line voltage is adopted as input power supply for the proposed audio amplifier system. In order to reduce the input voltage ripple, a smoothing capacitor C_{in} is parallel with rectified line voltage.

For a 200-W class-D audio amplifier system, when modulation index $m = 1$, the minimum bus voltages of the half-bridge class-D audio amplifier should satisfy

$$\left(\frac{V_{C3,\min}}{\sqrt{2}} \right)^2 / R_{speaker} \geq P_{out}. \quad (24)$$

According to [37], the peak-peak ripple voltage across capacitor C_{in} is

$$\Delta V_{in,pp} = \frac{P_{out}}{2\sqrt{2}f_{in}C_{in}V_{ac}}. \quad (25)$$

TABLE I
COMPARISON BETWEEN THE PROPOSED DCX AND SOME FRONT-END DC-DC CONVERTERS OF THE HALF-BRIDGE CLASS-D AUDIO AMPLIFIER

References	Flyback in [8]	VDRBHB in [10]	Bidirectional DC-DC converter in [17]	Bidirectional LLC converter in [28]	LLC DCX in [32]	LLC DCX in [34]	Proposed DCX
Switch	1	2	8	8	10	4	4
Diode	2	4	0	0	0	0	2
Inductor	0	2	1	2	0	1	0
Transformer	1	1	1	1	1	1	1
Controller	Complex	Complex	Complex	Complex	Simple	Simple	Simple
Output capacitor of the DC-DC converter	1000 μF	470 μF	-	-	-	440 μF	20 μF
Bidirectional power flowing	No	No	Yes	Yes	Yes	Yes	Yes
Soft switching in forward / backward mode	No / No	Yes / No	Yes / Yes	Yes / Yes	Yes / No	Yes / No	Yes / Yes
Input / output voltage	110 V/48 V	12 V/ ± 18 V	500 V/250 V	75~130 V/400 V	380 V/12 V	400 V/12 V	311 V/ ± 54 V
Switching frequency	25 kHz	100 kHz	100 kHz	69 kHz~92 kHz	1 MHz	530 kHz	200 kHz
Output power	100 W	60 W	1 kW	1 kW	800 W	300 W	200 W
Efficiency	84.04%	88.3%	98.2%	97.1%	97.6%	97.7%	96.3%

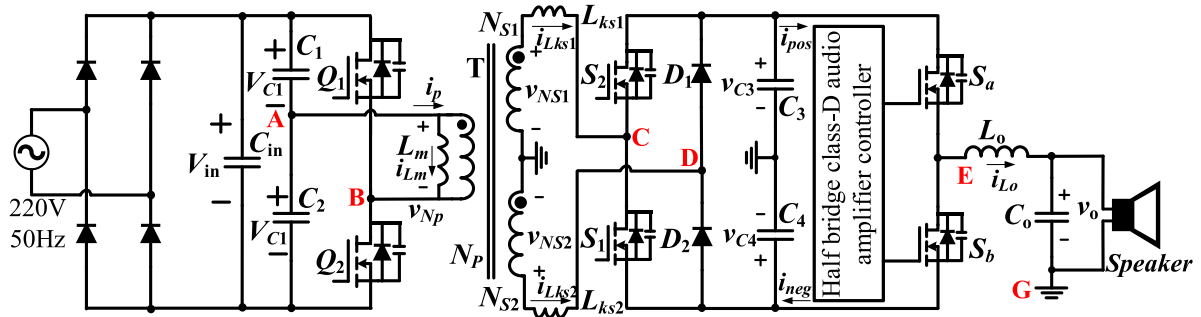


Fig. 18. Circuit diagram of the proposed half-bridge class-D audio amplifier system.

When the input voltage is minimal, (24) should be satisfied. The minimal input voltage is

$$V_{in,min} = (1 - 20\%) \cdot \sqrt{2}V_{ac} - \Delta V_{in,pp}/2. \quad (26)$$

When $V_{ac} = 220$ V, $P_{out} = 200$ W, $R_{speaker} = 4 \Omega$, $f_{in} = 50$ Hz, from (23) and (24)–(26), it has

$$C_{in} > 198.04 \mu\text{F}. \quad (27)$$

In this paper, $C_{in} = 220 \mu\text{F}$ is selected.

The specifications and circuit parameters are given in Table II.

Fig. 19(a) shows output voltage, positive and negative bus voltage of audio amplifier by using the converter in [10] as the front-end dc-dc converter, with $V_{pos} = -V_{neg} = 34$ V, $f_0 = 20$ Hz, $R_{load} = 8 \Omega$, $C_{pos} = C_{neg} = 50 \mu\text{F}$ and $v_o = 13.5$ V ac. It can be observed that the ripple of the bus voltages is large.

Fig. 19(b) shows output voltage, positive and negative bus voltage of audio amplifier by using the proposed DCX as the front-end converter, with $V_{C3} = -V_{C4} = 54$ V, $R_{load} = 8 \Omega$, $C_3 = C_4 = 20 \mu\text{F}$ and $v_o = 13.5$ V ac. It can be observed that the ripple of the bus voltages in the proposed DCX is much smaller than that in [10]. The results verify that the proposed

TABLE II
SPECIFICATIONS AND CIRCUIT PARAMETERS

	Output power, P_o	200 W
	Input Voltage, V_{in} / Output Voltage, V_{out}	Nominal 311 V / ± 54 V
	Switching Frequency, f_s	200 kHz
	Capacitors C_{in}	220 μF
	Capacitors C_{1-C_2} / C_{3-C_4}	1 μF / 20 μF
	Dead time $t_{d1}=t_{d2}$ / delay time $t_{d3}=t_{d4}$	60 ns / 100 ns
Transformer	$N_p : N_{S1} : N_{S2}$	20: 7: 7
	Magnetizing inductance L_m	85.1 μH
	Leakage inductances $L_{ks1}=L_{ks2}=L_k$ (transferred to secondary side)	0.35 μH
	Primary side switches Q_1 and Q_2	FDPF20N50FT
	Secondary side switches S_1 and S_2	TPH1500CNH
	Secondary side diodes D_1 and D_2	ES3DB

DCX eliminates the power supply pumping of the half-bridge class-D audio amplifier with small DCX output capacitors.

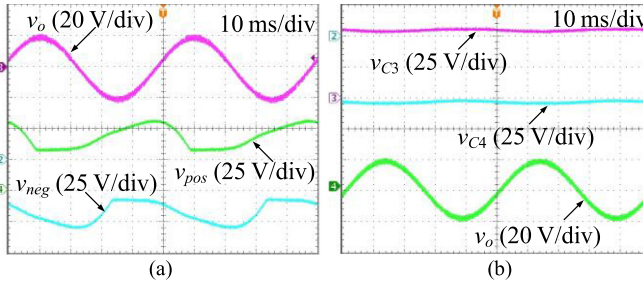


Fig. 19. Experimental waveforms of positive and negative bus voltage and audio amplifier output voltage with 8Ω load. (a) Unidirectional converter in [10] with $V_{pos} = -V_{neg} = 34$ V, $f_o = 20$ Hz, $C_{pos} = C_{neg} = 500 \mu\text{F}$ and $v_o = 13.5$ V ac. (b) Proposed DCX with $V_{C3} = -V_{C4} = 54$ V, $f_o = 20$ Hz, $C_3 = C_4 = 20 \mu\text{F}$ and $v_o = 13.5$ V ac.

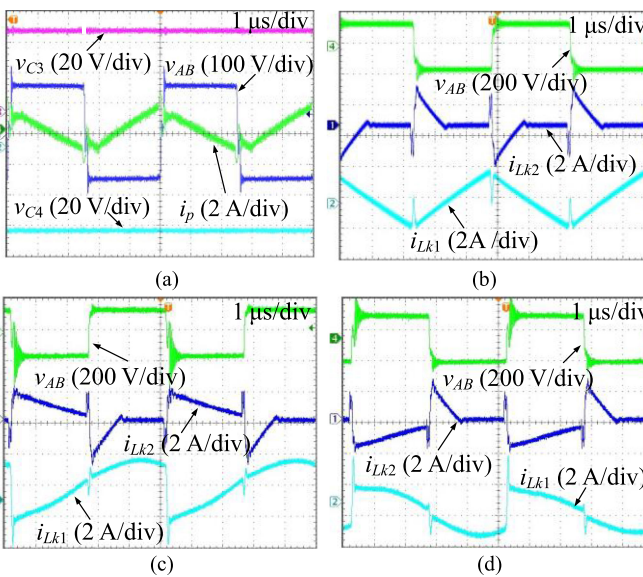


Fig. 20. Experimental waveforms of the proposed DCX connected half-bridge class-D audio amplifier. (a) Primary current i_p , positive and negative bus voltage V_{C3} and V_{C4} , and the voltage across transformer primary v_{AB} . (b) Currents i_{LK1} and i_{LK2} when the half-bridge class-D audio amplifier is light load, and the voltage across transformer primary v_{AB} . (c) Currents i_{LK1} and i_{LK2} when the half-bridge class-D audio amplifier is heavy load and load current i_{load} is positive, and the voltage across transformer primary v_{AB} . (d) Currents i_{LK1} and i_{LK2} when the half-bridge class-D audio amplifier is heavy load and load current i_{load} is negative, and the voltage across transformer primary v_{AB} .

Fig. 20(a) shows primary current i_p , positive and negative bus voltage V_{C3} and V_{C4} , and transformer primary voltage v_{AB} of the proposed DCX connected half-bridge class-D audio amplifier. Fig. 20(b)–(d) shows transformer primary voltage v_{AB} as well as currents i_{LK1} and i_{LK2} , when the half-bridge class-D audio amplifier operates at light load, positive heavy load, and negative heavy load.

Fig. 21(a)–(l) shows drain-source voltage V_{DS} and gate-source voltage V_{GS} of the MOSFETs in the proposed DCX when load current is positive, zero, and negative. It can be observed that ZVS turn-ON of switches Q_1 – Q_2 and S_1 – S_2 are realized.

Fig. 22(a) and (b) shows the dynamic performance of the proposed audio amplifier system with a 8Ω resistive load, under

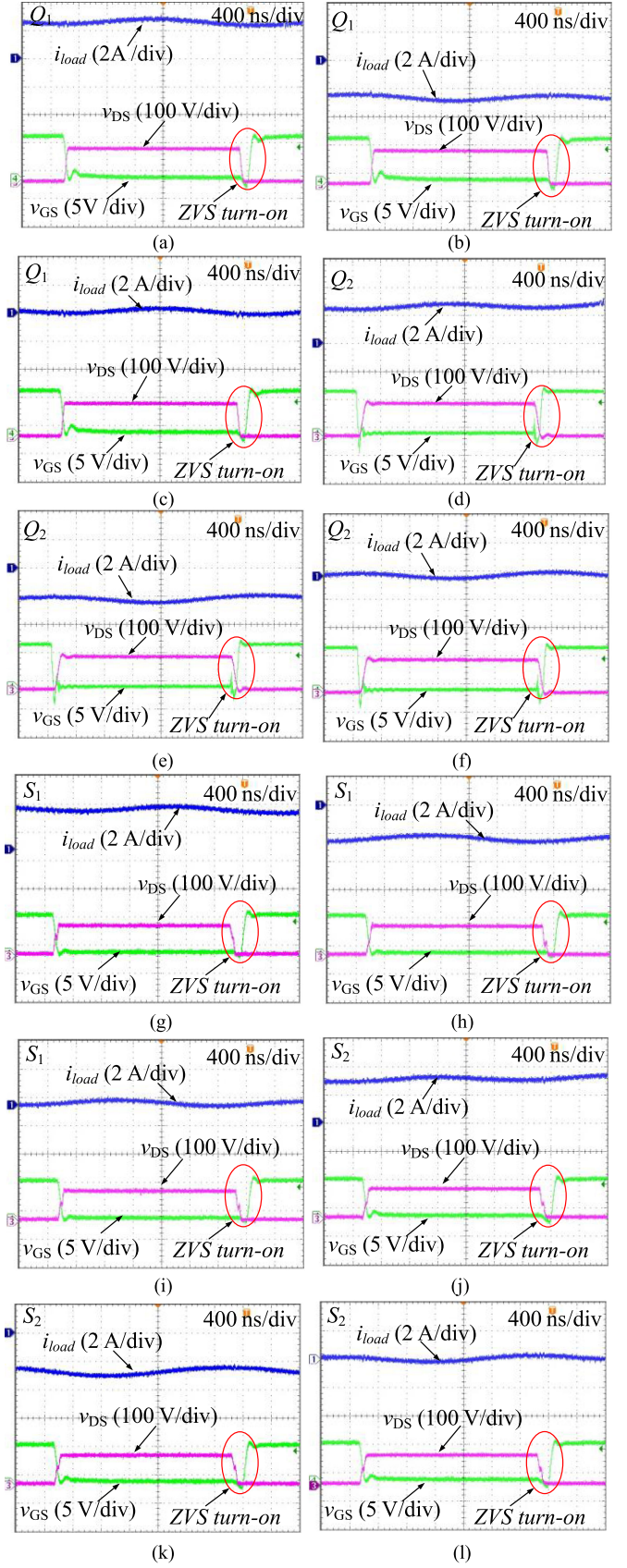


Fig. 21. Waveforms of v_{DS} and v_{GS} of MOSFETs in the proposed DCX.

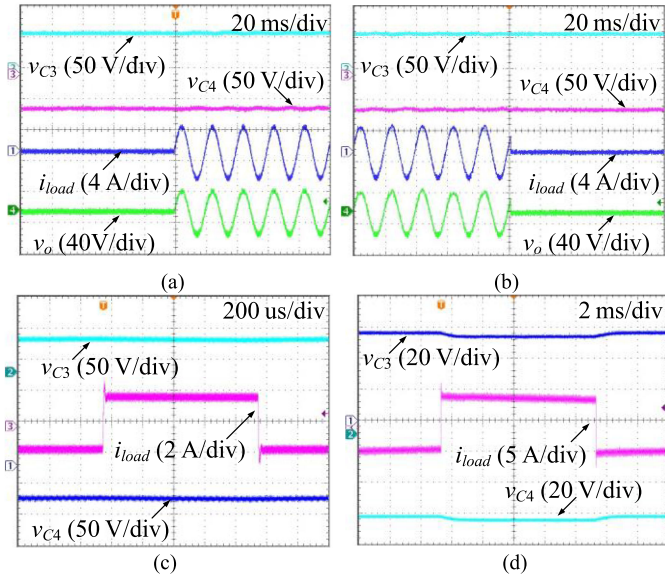


Fig. 22. Dynamic performance of the proposed DCX connected half-bridge class-D audio amplifier with resistive load. (a) Step load increase from 0 A to 2.5 A for 50 Hz sinusoidal audio amplifier output frequency. (b) Step load decrease from 2.5 A to 0 A for 50 Hz sinusoidal audio amplifier output frequency. (c) Step load between 2 A and -2 A for 500 Hz square audio amplifier output frequency. (d) Step load between 4 A and -4 A for 50 Hz square audio amplifier output frequency.

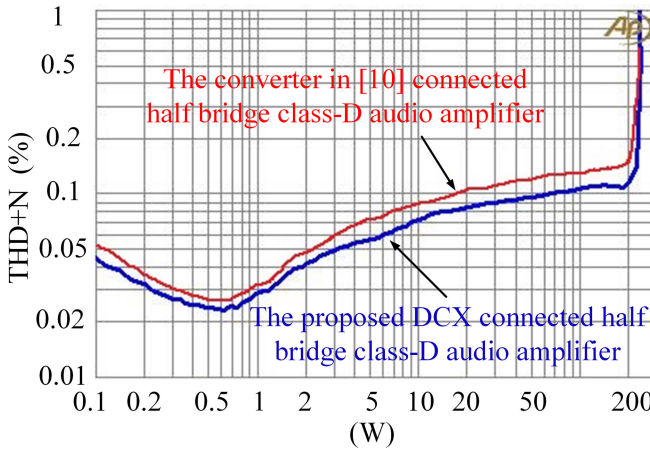


Fig. 23. Audio amplifier output voltage THD+N versus output power of the proposed DCX and the converter in [10] connected half-bridge class-D audio amplifier.

step load variation from 0 A to 2.5 A, and from 2.5 A to 0 A, with the frequency of the audio amplifier output sinusoidal voltage is 50 Hz. As shown in Fig. 22(a) and (b), the output voltages of the proposed DCX are constant under step load variation of the class-D audio amplifier, which reduces power supply pumping of the half-bridge class-D audio amplifier with a small output capacitor of the DCX. Fig. 22(c) shows the dynamic performance of the proposed audio amplifier system with a 4- Ω resistive load, under step load variation from -2A to 2A, and from 2A to -2A, with the frequency of audio amplifier output square voltage is 50 Hz. Fig. 22(d) shows the dynamic performance of the proposed audio amplifier system with a 4- Ω

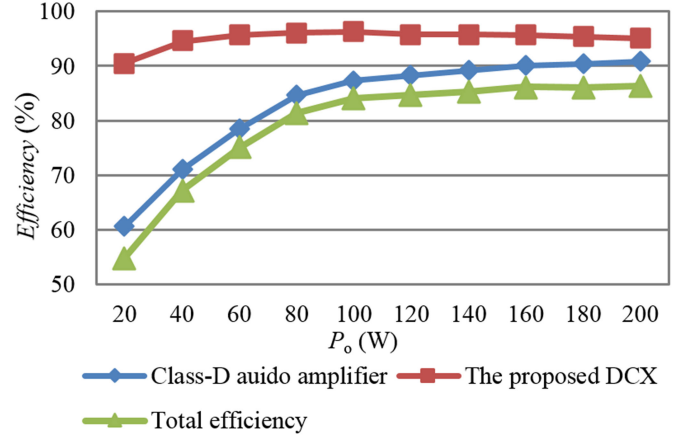


Fig. 24. Measured efficiency.

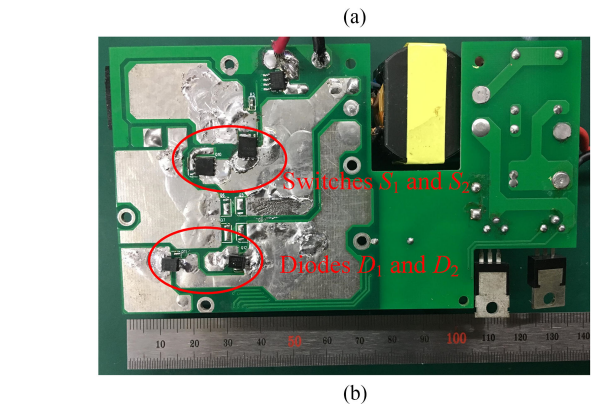
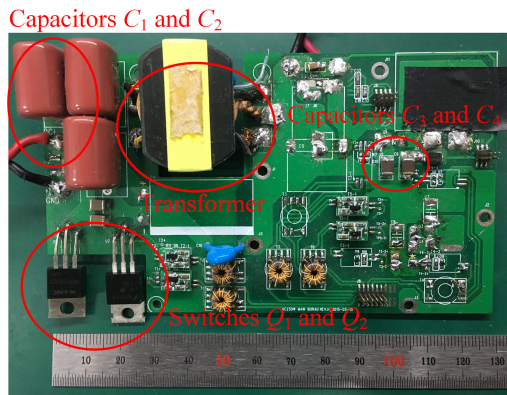


Fig. 25. Prototype of the proposed DCX. (a) Power board (Top). (b) Power board (Bottom).

resistive load, under step load variation from -4A to 4A, and from 4A to -4A, with the frequency of audio amplifier output square voltage is 50 Hz. As shown in Fig. 22(c) and (d), the bipolar outputs voltages of the proposed DCX are smoothing and stable relatively.

By using audio analyzer (Audio Precision 515), Fig. 23 shows the output voltage THD+N of the audio amplifier system with the proposed DCX and with the converter in [10] under different output power at 20 Hz output voltage frequency with a 4- Ω resistor load. From Fig. 23, output voltage THD+N of the half-bridge class-D audio amplifier with the proposed DCX is lower

than that with the converter in [10] because the proposed DCX eliminates the power supply pumping of the half-bridge class-D audio amplifier.

Fig. 24 shows the measured efficiency of the proposed converter. It can be observed that the highest efficiency is 96.3% at 100 W load, and the efficiency is higher than 95% over a wide load range. The proposed DCX idle loss is 2.15 W, and class-D idle loss is 4.42 W. Fig. 25 shows the prototype of the proposed DCX.

V. CONCLUSION

A soft switching symmetric bipolar outputs dc-transformer (DCX) for eliminating power supply pumping of half-bridge class-D audio amplifiers is proposed. Power supply pumping of the half-bridge class-D audio amplifier is eliminated by using the proposed DCX as a front-end dc-dc converter. Compared with using a bulk electrolytic capacitor to reduce the power supply pumping and voltage stress of the half-bridge class-D audio amplifier, the proposed DCX only need small output capacitors, and thus the power density of the audio amplifier system is improved. The proposed DCX provides stable symmetric bipolar output voltages bus with small switching ripple for the half-bridge class-D audio amplifier. In addition, the proposed DCX has smoothing transition between the positive load current and negative load current with a simple open-loop controller. ZVS turn-on of all the switches can be realized under ac load current, and thus high system efficiency is achieved in the proposed DCX.

REFERENCES

- [1] X. Jiang, "Fundamentals of audio class D amplifier design: A review of schemes and architectures," *IEEE Solid-State Circuits Mag.*, vol. 9, no. 3, pp. 14–25, Summer 2017.
- [2] M. A. Rojas-González and E. Sánchez-Sinencio, "Low-power high-efficiency class D audio power amplifiers," *IEEE J. Solid-State Circuits*, vol. 44, no. 12, pp. 3272–3284, Dec. 2009.
- [3] IRAUDAMP7D, "25 W-500 W scalable output power class D audio power amplifier reference design using the IRS2092 protected digital audio driver," 2008. [Online]. Available: <https://www.infineon.com>
- [4] B. Cordell, *Designing Audio Power Amplifiers*. New York, NY, USA: McGraw Hill, 2010, ch 29.5.
- [5] M. Berkhouit, L. Dooper, and B. Krabbenborg, "A 4Ω 2.65 W class-d audio amplifier with embedded DC-DC boost converter, current sensing ADC and DSP for adaptive speaker protection," *IEEE J. Solid-State Circuits*, vol. 48, no. 12, pp. 2952–2961, Dec. 2013.
- [6] S.-H. Chen *et al.*, "Embedded single-inductor bipolar-output DC-DC converter in class-D amplifier for low common noise," *IEEE Trans. Power Electron.*, vol. 31, no. 4, pp. 3106–3117, Apr. 2016.
- [7] X. Branca, B. Allard, X. Lin-Shi, and D. Chesneau, "Single-inductor bipolar-outputs converter for the supply of audio amplifiers in mobile platforms," *IEEE Trans. Power Electron.*, vol. 28, no. 9, pp. 4248–4259, Sep. 2013.
- [8] Y.-J. Tu, T.-L. Jong, and C.-M. Liaw, "Development of a class-D audio amplifier with switch-mode rectifier front-end and its waveform control," *IET Power Electron.*, vol. 4, no. 4, pp. 1002–1014, 2011.
- [9] IRAUDPS3-30 V, "+/-30 V power supply for class-D audio amplifier reference design user guide," 2015. [Online]. Available: <https://www.infineon.com>
- [10] C.-E. Kim, G.-W. Moon, and S.-K. Han, "Voltage doubler rectified boost-integrated half bridge (VDRBHB) converter for digital car audio amplifiers," *IEEE Trans. Power Electron.*, vol. 22, no. 6, pp. 2321–2330, Nov. 2007.
- [11] D. Nielsen, "Class D audio amplifiers for high voltage capacitive transducers," Ph.D. dissertation, Tech. Univ. Denmark, Lyngby, Denmark, 2014.
- [12] Self Douglas, *Audio Power Amplifier Design*. New York, NY, USA: Taylor & Francis, 2013.
- [13] T. Ge and J. S. Chang, "Bang-bang control class D amplifiers: Total harmonic distortion and supply noise," *IEEE Trans. Circuits Syst. I, Reg. Pap.*, vol. 56, no. 10, pp. 2353–2361, Oct. 2009.
- [14] A. I. Colli-Menchí, J. Torres, and E. Sánchez-Sinencio, "A feed-forward power-supply noise cancellation technique for single-ended class-D audio amplifiers," *IEEE J. Solid-State Circuits*, vol. 49, no. 3, pp. 718–728, Mar. 2014.
- [15] W. Shu and J. S. Chang, "Power supply noise in analog audio class D amplifiers," *IEEE Trans. Circuits Syst. I, Reg. Pap.*, vol. 56, no. 1, pp. 84–96, Jan. 2009.
- [16] S. Zhong, J. Xu, and X. Zhou, "2.1-channel switching amplifier with DC/high-frequency-ac mixed power supply for efficiency improvement and bus voltage pumping elimination," *IEEE Trans. Power Electron.*, vol. 33, no. 11, pp. 9110–9115, Nov. 2018, doi: [10.1109/TPEL.2018.2815742](https://doi.org/10.1109/TPEL.2018.2815742).
- [17] Y. Shen, H. Wang, A. Al-Durra, Z. Qin, and F. Blaabjerg, "A bidirectional resonant DC-DC converter suitable for wide voltage gain range," *IEEE Trans. Power Electron.*, vol. 33, no. 4, pp. 2957–2975, Apr. 2018.
- [18] H. Wu, S. Ding, K. Sun, L. Zhang, Y. Li, and Y. Xing, "Bidirectional soft-switching series-resonant converter with simple PWM control and load-independent voltage-gain characteristics for energy storage system in DC microgrids," *IEEE J. Emerg. Sel. Top. Power Electron.*, vol. 5, no. 3, pp. 995–1007, Sep. 2017.
- [19] H. Wu, K. Sun, Y. Li, and Y. Xing, "Fixed-frequency PWM-controlled bidirectional current-fed soft-switching series-resonant converter for energy storage applications," *IEEE Trans. Ind. Electron.*, vol. 64, no. 8, pp. 6190–6201, Aug. 2017.
- [20] K. Xiangli, S. Li, and K. M. Smedley, "Decoupled PWM plus phase-shift control for a dual-half-bridge bidirectional DC-DC converter," *IEEE Trans. Power Electron.*, vol. 33, no. 8, pp. 7203–7213, Aug. 2018, doi: [10.1109/TPEL.2017.2758398](https://doi.org/10.1109/TPEL.2017.2758398).
- [21] B. Zhao, Q. Song, W. Liu, and Y. Sun, "Overview of dual-active-bridge isolated bidirectional DC-DC converter for high-frequency-link power-conversion system," *IEEE Trans. Power Electron.*, vol. 29, no. 8, pp. 4091–4106, Aug. 2014.
- [22] Z. Hu, L. Wang, H. Wang, Y.-F. Liu, and P. C. Sen, "An accurate design algorithm for LLC resonant converters—Part I," *IEEE Trans. Power Electron.*, vol. 31, no. 8, pp. 5435–5447, Aug. 2016.
- [23] H.-Y. Yoon, H.-S. Lee, S.-H. Ham, H.-J. Choe, and B. Kang, "Off-time control of LLC resonant half-bridge converter to prevent audible noise generation at a light load condition," *IEEE Trans. Power Electron.*, vol. 33, no. 10, pp. 8808–8817, Oct. 2018, doi: [10.1109/TPEL.2017.2774840](https://doi.org/10.1109/TPEL.2017.2774840).
- [24] C. Fei, Q. Li, and F. C. Lee, "Digital implementation of adaptive synchronous rectifier (SR) driving scheme for high-frequency LLC converters with microcontroller," *IEEE Trans. Power Electron.*, vol. 33, no. 6, pp. 5351–5361, Jun. 2018.
- [25] C. Fei, F. C. Lee, and Q. Li, "Digital implementation of soft start-up and short-circuit protection for high-frequency LLC converters with optimal trajectory control (OTC)," *IEEE Trans. Power Electron.*, vol. 32, no. 10, pp. 8008–8017, Oct. 2017.
- [26] C. Fei, Y. Yang, Q. Li, and F. C. Lee, "Shielding technique for planar matrix transformers to suppress common-mode EMI noise and improve efficiency," *IEEE Trans. Ind. Electron.*, vol. 65, no. 2, pp. 1263–1272, Feb. 2018.
- [27] J.-H. Jung, H.-S. Kim, M.-H. Ryu, and J.-W. Baek, "Design methodology of bidirectional CLLC resonant converter for high-frequency isolation of DC distribution systems," *IEEE Trans. Power Electron.*, vol. 28, no. 4, pp. 1741–1755, Apr. 2013.
- [28] T. Jiang, J. Zhang, X. Wu, K. Sheng, and Y. Wang, "A bidirectional LLC resonant converter with automatic forward and backward mode transition," *IEEE Trans. Power Electron.*, vol. 30, no. 2, pp. 757–770, Feb. 2015.
- [29] J. Zhang, J. Liu, J. Yang, N. Zhao, Y. Wang, and T. Zheng, "A LLC-LC type bidirectional control strategy for LLC resonant converter in power electronic traction transformer," *IEEE Trans. Ind. Electron.*, vol. 65, no. 11, pp. 8595–8604, Feb. 2015, doi: [10.1109/TIE.2018.2808917](https://doi.org/10.1109/TIE.2018.2808917).
- [30] C. Fei, M. H. Ahmed, F. C. Lee, and Q. Li, "Two-stage 48 V-12 V/6 V-1.8 V voltage regulator module with dynamic bus voltage control for light-load efficiency improvement," *IEEE Trans. Power Electron.*, vol. 32, no. 7, pp. 5628–5636, Jul. 2017.
- [31] M. H. Ahmed, C. Fei, F. C. Lee, and Q. Li, "48-V voltage regulator module with PCB winding matrix transformer for future data centers," *IEEE Trans. Power Electron.*, vol. 64, no. 12, pp. 9302–9310, Dec. 2017.

- [32] C. Fei, F. C. Lee, and Q. Li, "High-efficiency high-power-density *LLC* converter with an integrated planar matrix transformer for high-output current applications," *IEEE Trans. Ind. Electron.*, vol. 64, no. 11, pp. 9072–9082, Nov. 2017.
- [33] M. Mu and F. C. Lee, "Design and optimization of a 380–12 V high-frequency, high-current *LLC* converter with GaN devices and planar matrix transformers," *IEEE J. Emerg. Sel. Top. Power Electron.*, vol. 4, no. 3, pp. 854–862, Sep. 2016.
- [34] W. Feng, P. Mattavelli, and F. C. Lee, "Pulsewidth locked loop (PWLL) for automatic resonant frequency tracking in *LLC* DC-DC transformer (*LLC-DCX*)," *IEEE Trans. Power Electron.*, vol. 28, no. 4, pp. 1862–1869, Apr. 2013.
- [35] W. Qin, X. Wu, and J. Zhang, "Current-feed single-switch forward resonant DC transformer (DCX) with secondary diode-clamping," *IEEE Trans. Ind. Electron.*, vol. 64, no. 10, pp. 7790–7799, Oct. 2017.
- [36] W. Qin, X. Wu, and J. Zhang, "A family of DC transformer (DCX) topologies based on new ZVZCS cells with DC resonant capacitance," *IEEE Trans. Power Electron.*, vol. 32, no. 4, pp. 2822–2834, Apr. 2017.
- [37] S. Johannes, *Rectifier Circuits: Theory and Design*. New York, NY, USA: Wiley, 1965.



Xiang Zhou (S'16–M'18) was born in Shaanxi, China, in 1991. He received the B.S. degree in electrical engineering from Southwest Jiaotong University, Chengdu, China, in 2013, where he is currently working toward the Ph.D. degree in power electronics.

His current research interests include soft switching dc–dc converter and dc–ac converter topology.



Jianping Xu (M'09) received the B.S. and Ph.D. degrees in electronic engineering from the University of Electronics Science and Technology of China, Chengdu, China, in 1984 and 1989, respectively.

Since 1989, he has been with the School of Electrical Engineering, Southwest Jiaotong University, Chengdu, China, where he has been a Professor since 1995. From November 1991 to February 1993, he was with the Department of Electrical Engineering, University of Federal Defense Munich, Munich, Germany, as a Visiting Research Fellow. From February 1993 to July 1994, he was with the Department of Electrical Engineering and Computer Science, University of Illinois at Chicago, Chicago, IL, USA, as a Visiting Scholar. His research interests include the modeling, analysis, and control of power electronic systems.



Shu Zhong was born in Hunan, China, in 1990. He received the B.S. degree in electrical engineering from Southwest Jiaotong University, Chengdu, China, in 2012, where he is currently working toward the Ph.D. degree in power electronics.

His current research interests include modulation and control of dc–dc converters, high frequency link dc–ac converters and switching audio amplifiers.



Yan-Fei Liu (M'94–SM'97–F'13) received the bachelor's and master's degrees from Zhejiang University, Hangzhou, China, in 1984 and 1987, respectively, and the Ph.D. degree from Queen's University, Kingston, ON, Canada, in 1994.

He was a Technical Advisor with the Advanced Power System Division, Nortel Networks, Ottawa, ON, Canada, from 1994 to 1999. Since 1999, he has been with Queen's University, where he is currently a Professor with the Department of Electrical and Computer Engineering. He has authored more than

230 technical papers in the IEEE Transactions and conferences, and holds 25 U.S. patents. He is also a Principal Contributor for two IEEE standards. His current research interests include digital control technologies for high efficiency, fast dynamic response dc–dc switching converters and ac–dc converters with power factor correction, resonant converters and server power supplies, and LED drivers.

Dr. Liu is currently the Vice President of Technical Operations of IEEE Power Electronics Society (PELS, from 2017 to 2018). He serves as an Editor of IEEE JOURNAL OF EMERGING AND SELECTED TOPICS OF POWER ELECTRONICS (IEEE JESTPE) since 2013. He will be the General Chair of ECCE 2019 to be held in Baltimore, USA, in 2019. His major service to IEEE is listed below: a Guest Editor-in-Chief for the special issue of Power Supply on Chip of IEEE TRANSACTIONS ON POWER ELECTRONICS from 2011 to 2013; a Guest Editor for special issues of JESTPE: Miniaturization of Power Electronics Systems in 2014 and Green Power Supplies in 2016; as Co-General Chair of ECCE 2015 held in Montreal, Canada, in September 2015; the Chair of PELS Technical Committee (TC1) on Control and Modeling Core Technologies from 2013 to 2016; Chair of PELS Technical Committee (TC2) on Power Conversion Systems and Components from 2009 to 2012. He is a fellow of Canadian Academy of Engineering and recipient of Modeling and Control Achievement Awards from IEEE Power Electronics Society. He was also the recipient of the Premier's Research Excellence Award in 2000 in Ontario, Canada, and the Award of Excellence in Technology in Nortel in 1997.